Active Design of Diffuse Acoustic Fields in Enclosures

Wilkins Aquino, Jerry Rouse, Marc Bonnet

Active Design of Diffuse Acoustic Fields in Enclosures

Wilkins Aquino,[1, a] Jerry Rouse,[2] and Marc Bonnet[3]

[1]*Department of Mechanical Engineering and Materials Science, Duke University, Durham. NC, 27708, USA*

[2]*Analytical Structural Dynamics, Sandia National Laboratories, Albuquerque, New Mexico, 87123, USA*

[3]*POEMS (CNRS-ENSTA-INRIA), ENSTA Paris, Palaiseau, France*

This paper presents a numerical framework for designing diffuse fields in rooms of any shape and size, driven at arbitrary frequencies. That is, we aim at overcoming the Schroeder frequency limit for generating diffuse fields in an enclosed space. We formulate the problem as a Tikhonov regularized inverse problem and propose a low-rank approximation of the spatial correlation that results in significant computational gains. Our approximation is applicable to arbitrary sets of target points and allows us to produce an optimal design at a computational cost that grows only linearly with the (potentially large) number of target points. We demonstrate the feasibility of our approach through numerical examples where we approximate diffuse fields at frequencies well below the Schroeder limit.

[a]wilkins.aquino@duke.edu

I. INTRODUCTION

Many aerospace structures, satellites and internal components experience acoustic loads that are diffuse in nature. That is, these loads are composed of a large number of waves having random amplitude, propagation direction and phase. Ground-based qualification testing of these structures are typically performed in acoustic reverberation chambers within which a diffuse field arises naturally. The minimum frequency beyond which an acoustic field in an enclosure is (naturally) diffuse, termed the Schroeder frequency[1,2], depends on the chamber volume V and absorption as per the relation

$$f_s = \sqrt{\frac{c^3\, T_{60}}{4\ln(10) V}} \tag{1}$$

Here, c is the phase speed and T_{60} the reverberation time, the time required after source termination for the energy in the room to attenuate 60 dB. This expression provides an estimate of the frequency at which sufficient modal overlap first occurs. See Kuttruff[3] for a detailed derivation of (1).

The dimensions of a chamber determine the lowest frequency at which a diffuse field would naturally occur, as f_s^2 is inversely proportional to the enclosure volume. Although there are means to improve or fully develop a diffuse field within a given chamber such as splayed walls, rotating panels, and moving vanes[4], there are currently no known means to induce a diffuse field at frequencies below f_s.

Traditionally, large air horns were used to generate the necessary high amplitude acoustic levels within reverberation chambers. Recently, horns have been augmented or replaced with concert-grade loudspeakers, allowing improved closed-loop control and the potential

to achieve a wider range of test spectra[5,6]. The addition of loudspeaker sources provides an opportunity for optimizing the acoustic field within a chamber, as will be shown in this paper. Synthesizing diffuse fields below the Schroeder frequency can lead to significant financial and time savings. For instance, physical dimensions of new chambers could be relaxed and shipping of test articles across facilities could be eliminated.

The design of diffuse acoustic fields has been explored, to some extent, in the open literature. Specific examples include the work of Bravo and Maury[7] who designed various types of acoustic random fields, including diffuse fields, using direct acoustic field testing. To that end, they solved a quadratic optimization problem in which they found correlated sources that minimized the misfit between the predicted field and the spatial correlation of the target random field near the surface of a test body. In recent work, Alvarez-Blanco et al.[8] presented an approach to design controls for an array of loud speakers to create diffuse fields in direct acoustic tests. For this, they also used a pseudo-inverse strategy to obtain solutions of a quadratic optimization problem that directly provided the signal inputs. For other relevant, recent work in this area see[9–11].

As in the aforementioned work, we are interested in designing diffuse fields. However, in contrast to the existing literature, we investigate the synthesis of these fields in reverberant rooms at arbitrary frequencies (even below the Schroeder limit). Hence, our main contribution is the development of a numerical approach for the design of acoustic diffuse fields in enclosed rooms. To that end, we put forward a PDE-constrained optimization formulation for the control problem. Although existing work has addressed the Multiple Input Multiple Output (MIMO) control problem[7,8], we provide further insight into Tikhonov regularization

for these problems. Moreover, one of the numerical challenges in designing or producing samples of a diffuse field in simulations is the need to capture its spatial correlation. The latter may require fine discretizations (e.g. using finite elements) that lead to large dense matrices.

The computational challenge of factorizing the spatial correlation (in the context of diffuse fields) was recently addressed in[12], who proposed to generate diffuse fields given by expansions on the eigenfunctions of the pressure correlation operator (i.e. using the Karhunen-Loève decomposition of the latter). To avoid the computational bottleneck of factorizing a dense correlation, they employed a low-order Taylor expansion in Cartesian components of the relative position vector, approximating the continuous correlation function while ensuring the vector does not exceed the operating wavelength significantly. This approximation reduced the correlation to a product of univariate kernels, whose eigenfunctions are recognized as spheroidal wave functions

In contrast, our approach exploits a more-accurate low-rank approximation of the correlation function, applicable to arbitrary sets of target points. This allows us to solve the least-squares problem producing an optimal design at a computational cost that grows only linearly with the (potentially large) number of target points (instead of quadratically if using directly the dense correlation matrix). In addition, this proposed treatment allows us to formulate simple and efficient regularized versions of the optimization problem, which cater to it being possibly ill-conditioned and remain computationally economical.

The rest of the paper is organized as follows. We provide a summary of the plane-wave model for diffuse fields and the ensuing statistics. We then formulate the forward problem

for modeling a random acoustic field in an enclosed room. Next, we provide the optimization formulation for the control problem and the description of our approach for the low-rank approximation of the spatial correlation. We also offer two Tikhonov regularization strategies for the control problem. Next, we demonstrate the feasibility of our proposed strategy using numerical examples in an enclosed room driven at frequencies below the Schroeder limit. Finally, we provide some conclusions and future directions.

II. BACKGROUND

Here we summarize existing results on the theoretical modeling of diffuse fields. We will adopt the plane wave model in which a random pressure field is conceived as the interaction of an infinite number of plane waves with randomized direction and phase[13]. It is well known that this model leads to a Gaussian spatio-temporal pressure field, which is fully characterized by its mean and correlation function. In this work, for the sake of simplicity and without loss of generality, we will concentrate on pure-tone fields.

A. Plane Wave Model

Following Jacobsen[14], we model a pure-tone diffuse field as a random pressure field expressed as

$$P(\boldsymbol{x},\omega;\theta) = \lim_{N\to\infty} \frac{1}{\sqrt{N}} \sum_{n=1}^{N} A_n e^{-i(\kappa \boldsymbol{D}_n\cdot\boldsymbol{x}+\boldsymbol{\Phi}_n)} \tag{2}$$

where $\kappa = \omega/c$ is the wave number, c is the speed of sound, $\boldsymbol{D}_n$ are independent random vectors (uniformly distributed over the unit sphere) describing the direction of a plane wave,

A_n are independent random variables, and Φ_n are random phases. The vector θ represents the collection of all the random variables in the model. Notice that, as a consequence of the Central Limit Theorem, the random field $P(\boldsymbol{x}, \omega; \theta)$ is Gaussian[14]. Also, without loss of generality, we use in the sequel a constant value $A_n := p_0$.

B. First and Second Order Statistics of a Diffuse Field

Here we summarize well-known results on the statistics of the stochastic field shown in (2). It is straightforward to show that

$$\mathbb{E}[P(\boldsymbol{x}, \omega; \theta)] = 0 \quad \forall \boldsymbol{x}, \omega$$

where $\mathbb{E}[\cdot]$ denotes expectation.

Let $r_{qs} = \|\boldsymbol{x}_q - \boldsymbol{x}_s\|$ be the distance between any two points $\boldsymbol{x}_q$ and $\boldsymbol{x}_s$. Then, the correlation can be shown to be given by[15]

$$\begin{aligned} G(r_{qs}, \omega) &= \mathbb{E}[P(\boldsymbol{x}_q, \omega; \theta)\overline{P}(\boldsymbol{x}_s, \omega; \theta)] \\ &= \frac{p_0^2}{2}\frac{\sin(\kappa(\omega) r_{qs})}{\kappa(\omega) r_{qs}} \end{aligned} \tag{3}$$

where the overbar denotes complex conjugation.

As previously noted, the random field $P(\boldsymbol{x}, \omega; \theta)$ is Gaussian. Hence, we can completely characterize the diffuse field through its mean and correlation. Moreover, the field is weakly isotropic (i.e. the mean is constant and the correlation depends only on the distance between two points)[16]. A more extensive discussion on diffuse fields can be found in[14,15,17,18].

III. DESIGN OF DIFFUSE FIELDS

As stated before, we seek to develop a numerical framework for designing approximately diffuse fields for rooms of any shape and size at arbitrary frequencies. To this end, we first introduce the acoustic equations and numerical approximations, followed by the design problem, and a formal regularized treatment of the ensuing ill-posed design problem.

As we will see later in this section, one of the key challenges in the design problem is the computational expense that arises from the discretization of the target correlation function. One of our contributions in this work is an efficient low-rank representation of the target correlation that renders the design problem tractable.

A. Forward Problem

We model a room as a bounded domain $\Omega \subset \mathbb{R}^3$ with boundary (walls) Γ. The part of the walls with impedance conditions is denoted as Γ_r, while that occupied by the speakers is denoted as $\Gamma_N = \cup_j \Gamma_{N_j}, j = 1 \dots d$, where d is the number of speakers in the room and $\Gamma = \Gamma_r \cup \Gamma_N$. The pressure field in the room satisfies[19]

$$\begin{aligned} \nabla^2 p + \kappa^2 p &= 0 \quad \text{in } \Omega \\ \nabla p \cdot \boldsymbol{n} + \mathrm{i} Z^{-1} \omega \rho_0 p &= 0 \quad \text{on } \Gamma_r \\ \nabla p \cdot \boldsymbol{n}_j - \rho_0 s_j &= 0 \quad \text{on } \Gamma_{N_j} \quad \text{for } j = 1, \dots, d \end{aligned} \tag{4}$$

where ω is the angular frequency, ρ_0 is the fluid density, κ is the wavenumber, s_j is the normal acoustic acceleration over Γ_j, Z is the specific acoustic impedance, and $\boldsymbol{n}_j$ is a unit vector normal to Γ_j and directed out of the room. Using the Finite Element Method[20] to

obtain a discrete representation of (4), we arrive at

$$R\boldsymbol{p} = F\boldsymbol{s}$$

where $R := K - \kappa^2 M + \mathrm{i}\omega C$, K is the acoustic stiffness, M is the mathematical mass matrix, C is the damping matrix, $F \in \mathbb{R}^{N\times d}$ is a matrix that acts on the acoustic accelerations vector $\boldsymbol{s} \in \mathbb{R}^d$.

Let $\mathcal{T} := \left\{\boldsymbol{x}_1, \ldots, \boldsymbol{x}_m\right\}$ be a finite set of m target locations where we want the field to be diffuse. Now, let $B \in \mathbb{R}^{m\times d}$ be the Boolean matrix such that $\boldsymbol{p}_\mathcal{T} = B\boldsymbol{p} \in \mathbb{C}^m$ collects the nodal pressures at the target locations. We then have

$$\begin{aligned}\boldsymbol{p}_\mathcal{T} &= B\boldsymbol{p}\\ &= BR^{-1}F\boldsymbol{s}\\ &= T\boldsymbol{s}\end{aligned}$$

where we have introduced the transfer matrix $T := BR^{-1}F \in \mathbb{C}^{m\times d}$. Also, we point out that if $Z \neq 0$, R is invertible for any frequency[21].

For random sources, the relationship between the cross-correlation of the target pressures denoted as G, and the cross-correlation of the sources, denoted as S, at a given frequency is given as

$$\begin{aligned}G &= \mathbb{E}\left[\boldsymbol{p}_\mathcal{T}\boldsymbol{p}_\mathcal{T}^h\right]\\ &= T\,\mathbb{E}\left[\boldsymbol{s}\boldsymbol{s}^h\right]T^h\\ &= TST^h\end{aligned} \tag{5}$$

where the superscript h denotes complex conjugation and transposition. So, given S, we can compute G at given locations. Next, we develop a design methodology for diffuse fields based on the forward model presented in this section.

B. Inverse or Design Problem

Our design problem can be described as: given a cross-correlation at a set $\mathcal{T}$ of target nodes, determine the cross-correlation of the input sources. To this end, let $\boldsymbol{x}_i, \boldsymbol{x}_j \in \mathcal{T}$ be two target locations. Then, from (3), the components of the target cross-correlation matrix at a given frequency, $\hat{G}_{ij}$, are given as

$$\hat{G}_{ij} = \frac{p_o^2}{2} \frac{\sin(\kappa r_{ij})}{\kappa r_{ij}} \tag{6}$$

We first introduce an un-regularized inverse problem for the sake of simplicity. This formulation leads to a decomposition of the inverse problem that strongly reduces computational cost, as will be shown. After this, a regularized version of the problem follows naturally. Define an objective function as

$$J(S) := \frac{1}{2} \|G(S) - \hat{G}\|_F^2 \tag{7}$$

where $G(S)$ solves (5) and $\|G\|_F$ is the Frobenius matrix norm, which is associated with an inner product: $\|G\|_F^2 = (G, G)_F =: \operatorname{tr}\left(G^h G\right)$. Then, the optimal cross-correlation, S_o, can be obtained as

$$S_o = \underset{S \in \mathbb{C}^{d \times d}}{\arg\min}\, J(S). \tag{8}$$

While the search space for the above minimization should *a priori* be restricted to positive definite and Hermitian matrices S, it turns out that the minimum-norm solution found by the unconstrained minimization (8) automatically satisfies those requirements, see Remark 3.

C. Optimality Condition and minimum-norm least-squares solution

To simplify our derivations, define a linear operator $\mathcal{A} : \mathbb{C}^{d\times d} \to \mathbb{C}^{m\times m}$ as

$$\mathcal{A}S := TST^h \tag{9}$$

Substituting this expression into the objective (7), we get

$$J(S) := \frac{1}{2}\|\mathcal{A}S - \hat{G}\|_F^2$$

The first-order optimality condition for Problem (8) is that the gradient of the objective be zero at the minimizer. Using the inner product associated with the Frobenius norm, the directional derivative of the objective at $S \in \mathbb{C}^{d\times d}$ in an arbitrary direction $H \in \mathbb{C}^{d\times d}$ is obtained as

$$\begin{aligned}\langle J'(S), H\rangle &= \frac{d}{d\epsilon} J(S+\epsilon H)\Big|_{\epsilon=0} \\ &= \mathrm{Re}\big(\mathcal{A}S - \hat{G}, \mathcal{A}H\big)_F \\ &= \mathrm{Re}\big(\mathcal{A}^\star\mathcal{A}S - \mathcal{A}^\star\hat{G}, H\big)_F\end{aligned}$$

where $\mathcal{A}^\star$ denotes the adjoint of $\mathcal{A}$, defined by $(W, \mathcal{A}V)_F = (\mathcal{A}^\star W, V)_F$ for any $W \in \mathbb{C}^{m\times m}$ and $V \in \mathbb{C}^{d\times d}$. Then, from the above expression, the first-order optimality condition $J'(S_o) = 0$ verified by S_o is obtained as

$$\mathcal{A}^\star\mathcal{A}S_o - \mathcal{A}^\star\hat{G} = 0, \tag{10}$$

which is in essence the normal equation for the least squares problem (8). Then, using (9) in (10) and simplifying, we get

$$T^h T S_o T^h T = T^h \hat{G} T$$

If $T^h T$ is not invertible (i.e. if T does not have full column rank d), the above equation fails to provide a solution $S_o \in \mathbb{C}^{d\times d}$ that is invertible (let alone positive definite). The transfer matrix T is therefore assumed henceforth to have rank d.

To solve equations (10), and also to later address regularized versions of Problem (8), it is convenient and computationally reasonable (under the present operating conditions) to introduce and use the reduced singular value decomposition (SVD) of T:

$$T = X\Sigma Y^h, \tag{11}$$

where $\Sigma \in \mathbb{R}^{d\times d}$ is a diagonal matrix holding the d nonzero singular values $\sigma_1 \geq \sigma_2 \geq \ldots \sigma_d > 0$ of T while $X \in \mathbb{C}^{m\times d}$ and $Y \in \mathbb{C}^{d\times d}$ hold the d left and right associated singular vectors (arranged columnwise), respectively. In particular, the matrices X and Y have the orthonormality properties $X^h X = I_d$ and $Y^h Y = Y Y^h = I_d$, with I_d the $d \times d$ identity matrix. On introducing the SVD (11) in (10) and using the latter properties of X and Y, the minimum-norm least-squares solution S_o is found as

$$S_o = Y\Sigma^{-1}(X^h \hat{G} X)\Sigma^{-1} Y^h. \tag{12}$$

and is clearly Hermitian and positive definite. Moreover, for any $\boldsymbol{s} \in \mathbb{C}^d$, we have $\boldsymbol{s}^h S_o \boldsymbol{s} = (X\Sigma^{-1}Y^h\boldsymbol{s})^h \, \hat{G} \, (X\Sigma^{-1}Y^h\boldsymbol{s}) > 0$ by virtue of the positive definiteness of $\hat{G}$, showing that S_o is in fact positive definite.

The expression (12) of S_o entails the evaluation of $X^h\hat{G}X$, whose $O(dm^2 + d^2m/2)$ cost constitutes a potential computational bottleneck as $\hat{G}$ is a dense $m \times m$ matrix that may be large in realistic problems (e.g. $m = O(10^4)$ to $O(10^6)$). To reduce the computational complexity in m of the design solution method, we now introduce a low-rank approximation of $\hat{G}$.

D. Low-rank approximation of $\hat{G}$

The target correlation $\hat{G}$ being symmetric and positive definite, we have $\hat{G} = \sum_{k=1}^{m} \boldsymbol{\psi}_k \boldsymbol{\psi}_k^h \lambda_k$, where $\boldsymbol{\psi}_k, \lambda_k$ are the eigenpairs of $\hat{G}$ numbered so that $\lambda_1 \geq \lambda_2 \ldots \geq \lambda_m > 0$. By the Eckart-Young theorem, this expansion, truncated to its first P terms, yields the best rank-P approximation of $\hat{G}$, denoted as $\hat{G}_P$, in the sense of the Frobenius norm. Specifically, the relative truncation error is given as

$$\mathcal{E}^2(P) := \frac{\|\hat{G} - \hat{G}_P\|_F^2}{\|\hat{G}\|_F^2} = \frac{\sum_{k=P+1}^{m} \lambda_k^2}{\sum_{j=1}^{m} \lambda_j^2} \tag{13}$$

The rate of decay of the eigenvalues of a correlation matrix depends on the correlation length. The latter is usually high, which allows a truncation order $Q \ll m$. However, setting up this approximation still entails obtaining a large enough number of eigenpairs of the $m \times m$ matrix $\hat{G}$ to achieve and verify a sufficiently low truncation error, and this remains often impractical.

We therefore propose an alternative strategy for deriving low-rank approximations of $\hat{G}$. It is based on observing that the generic entry $\hat{G}_{ij}$ of $\hat{G}$, see (6), is in fact equivalently given

as

$$\hat{G}_{ij} = \frac{p_o^2}{2} j_0(\kappa|\boldsymbol{r}_{ij}|)$$

where j_0 is the spherical Bessel function of first kind and order zero and $\boldsymbol{r}_{ij} := \boldsymbol{x}_i - \boldsymbol{x}_j$ is the position vector joining two generic target points. Now, for any $\boldsymbol{z} \in \mathbb{R}^3$, the function j_0 admits the integral representation

$$j_0(|\boldsymbol{z}|) = \frac{1}{4\pi} \int_{\widehat{S}} e^{\mathrm{i}\boldsymbol{z}\cdot\hat{\boldsymbol{\theta}}} \, \mathrm{d}S(\hat{\boldsymbol{\theta}}), \tag{14}$$

where $\widehat{S}$ is the unit sphere (spanned by unit vectors $\hat{\boldsymbol{\theta}}$). For instance, expressing the above integral using spherical angular coordinates reduces it to the one-dimensional integral representation formula (10.54.1) given in[22]. Let the above integral be approximated by a Q-point quadrature rule with nodes $\hat{\boldsymbol{\theta}}_q \in \widehat{S}$ and positive weights w_q $(1 \leq q \leq Q)$, yielding

$$j_0(|\boldsymbol{z}|) = \Big(\frac{1}{4\pi} \sum_{q=1}^{Q} w_q e^{\mathrm{i}\boldsymbol{z}\cdot\hat{\boldsymbol{\theta}}_q} \Big) + \varepsilon_Q,$$

ε_Q being the quadrature error. Setting $\boldsymbol{z} = \kappa(\boldsymbol{x}_i - \boldsymbol{x}_j)$, we thus approximate $\hat{G}_{ij}$ as

$$\hat{G}_{ij} \approx \frac{p_o^2}{8\pi} \sum_{q=1}^{Q} w_q e^{\mathrm{i}\boldsymbol{x}_i\cdot\hat{\boldsymbol{\theta}}_q} \, e^{-\mathrm{i}\boldsymbol{x}_j\cdot\hat{\boldsymbol{\theta}}_q},$$

a result which in turn yields, upon application to all pairs of target points, the following (approximate) decomposition of the target correlation matrix $\hat{G}$:

$$\hat{G} \approx \Phi\Phi^h = \sum_{q=1}^{Q} \boldsymbol{\phi}_q \boldsymbol{\phi}_q^h, \qquad \Phi = [\boldsymbol{\phi}_1, \ldots, \boldsymbol{\phi}_q] \in \mathbb{C}^{m\times Q}, \ \Phi_{jq} = (\boldsymbol{\phi}_q)_j = \sqrt{w_q} e^{\mathrm{i}\boldsymbol{x}_i\cdot\hat{\boldsymbol{\theta}}_q}. \tag{15}$$

The size Q of the quadrature rule ensuring a desired (small enough) quadrature error depends on the oscillatory character of the integral (14), and hence on the magnitude of the argument $|\boldsymbol{z}|$ of j_0 there. In this study, the latter is bounded from above by the largest spatial

separation between target points and the operating frequency. Consequently, Q does not depend on the number m of target points once their maximum spatial separation is fixed. In the forthcoming examples, $Q = O(10^2)$ whereas $m = O(10^4)$, so that (15) accomplishes a low-rank approximation of $\hat{G}$, whose computation is moreover economical as the m-vectors $\boldsymbol{\phi}_q$ are given explicitly.

The low-rank approximation (15) greatly reduces the computational load in evaluating S_o. Indeed, using (15) in (12) gives

$$S_o = (Y\Sigma^{-1}Z)(Y\Sigma^{-1}Z)^h, \qquad Z := X^h\Phi \in \mathbb{C}^{d\times Q},$$

whose evaluation needs only $O(m)$ computational work and memory, down from $O(m^2)$ if using the full matrix $\hat{G}$.

Remark 1 *Unlike in the expansion* $\hat{G} = \sum_{q=1}^{m} \boldsymbol{\psi}_q \boldsymbol{\psi}_q^T \lambda_q$ *in terms of eigenpairs, the vectors* $\boldsymbol{\phi}_q$ *in* (15) *are not orthogonal.*

E. Regularized least-squares solution

We now address the case where T^hT may be ill-conditioned (i.e. have a large condition number), with T still assumed to have full column rank. Let

$$\boldsymbol{s}_q = Y\Sigma^{-1}X^h\boldsymbol{\phi}_q \tag{16}$$

Then, the minimum-norm solution to (8) is given by

$$S_o = \sum_{q=1}^{Q} \boldsymbol{s}_q \boldsymbol{s}_q^h \tag{17}$$

We notice that $\boldsymbol{s}_q$ given by (16) is (by our assumption on T) the unique solution of the least-squares problem

$$\boldsymbol{s}_q = \arg\min_{\boldsymbol{u}\in\mathbb{C}^d} \frac{1}{2}\big\| T\boldsymbol{u} - \boldsymbol{\phi}_k \big\|_2^2 \tag{18}$$

where $\|\cdot\|_2$ is the Euclidean norm. Therefore, to obtain S_o given by (17), we have to solve at most Q problems of the type (18). To cater for T^hT being possibly ill-conditioned, we add a regularization term in (18) to get the problem

$$\boldsymbol{s}_q(\alpha) = \arg\min_{\boldsymbol{u}\in\mathbb{C}^d} \frac{1}{2}\Big(\big\| T\boldsymbol{u} - \boldsymbol{\phi}_q \big\|_2^2 + \alpha\|\boldsymbol{u}\|_2^2 \Big), \tag{19}$$

(where $\alpha > 0$ is a regularization parameter), whose unique minimizer is given in closed form as

$$\boldsymbol{s}_q(\alpha) = Y(\Sigma + \alpha\, I)^{-1} X^h \boldsymbol{\phi}_q. \tag{20}$$

The resulting input correlation matrix is then given by

$$S_{o1}(\alpha) := \sum_{q=1}^{Q} \boldsymbol{s}_q(\alpha)\boldsymbol{s}_q^h(\alpha) = \big(Y(\Sigma + \alpha\, I)^{-1} Z\big)\,\big(Y(\Sigma + \alpha\, I)^{-1} Z\big)^h. \tag{21}$$

We can show that $S_{o1}(\alpha)$ converges to the minimum-norm solution S_{o1} of our original problem (8) as $\alpha \to 0$. Indeed, from (16) and (20), we have

$$\begin{aligned}
\boldsymbol{s}_q(\alpha) - \boldsymbol{s}_q &= Y\big[(\Sigma + \alpha\, I)^{-1} - \Sigma^{-1}\big] X^h \boldsymbol{\phi}_q \\
&= Y(\Sigma + \alpha\, I)^{-1}\big[I - (\Sigma + \alpha\, I)\Sigma^{-1}\big] X^h \boldsymbol{\phi}_q \\
&= -\alpha Y(\Sigma + \alpha\, I)^{-1}\Sigma^{-1} X^h \boldsymbol{\phi}_q
\end{aligned}$$

Therefore, $\|\boldsymbol{s}_q(\alpha) - \boldsymbol{s}_q\| \to 0$ and $\|S_{o1}(\alpha) - S_o\|_F \to 0$ as $\alpha \to 0$ (since $S_{o1}(\alpha)$ and S_o are both given by finite sums of tensor products)

Second regularization method

Alternatively, we can consider the regularized version

$$S_{o2}(\alpha) := \arg\min_{S\in\mathbb{C}^{d\times d}} J_\alpha(S), \qquad J_\alpha(S) := \frac{1}{2}\|\mathcal{A}S - \hat{G}\|_F^2 + \frac{\alpha}{2}\|S\|_F^2 \tag{22}$$

of the original least-squares problem (8), whose stationarity condition is

$$T^h T S_{o2}(\alpha) T^h T + \alpha S_{o2}(\alpha) = T\hat{G}T^h.$$

Invoking again the reduced SVD (11) of T, the above equation becomes

$$\Sigma^2 H(\alpha)\Sigma^2 + \alpha H(\alpha) = \Sigma\hat{H}\Sigma, \qquad \text{with} \quad H := Y^h S_{o2}(\alpha) Y. \tag{23}$$

Since Σ is diagonal, the above equation decouples into componentwise scalar equations whereby

$$H_{ij}(\alpha) = \frac{\sigma_i\sigma_j}{\sigma_i^2\sigma_j^2 + \alpha}(ZZ^h)_{ij} \qquad 1 \le i, j \le d, \tag{24}$$

and $S_{o2}(\alpha) = YH(\alpha)Y^h$ is readily found once $H(\alpha)$ is evaluated using the above formula. Moreover, it is easy to verify that (24) with $\alpha = 0$ yields $S_o = YH(0)Y^h$ through (12), and that we have

$$H_{ij}(\alpha) - H_{ij}(0) = -\frac{\alpha}{\sigma_i\sigma_j(\sigma_i^2\sigma_j^2 + \alpha)}(ZZ^h)_{ij} \qquad 1 \le i, j \le d.$$

Consequently, this second regularization approach also verifies $\|S_{o2}(\alpha) - S_o\| \to 0$ as $\alpha \to 0$.

Remark 2 *The first regularization yields $H_{ij}(\alpha) = (ZZ^h)_{ij}/(\sigma_i+\alpha)(\sigma_j+\alpha)$ instead of (24), with H_{ij} as in (23). This shows that the two regularization approaches are not identical, although the next remarks 3, 4 show that they are similar in several ways.*

Remark 3 *The minimum-norm solution S_o to problem (8), as well as its regularized approximations $S_{o1}(\alpha)$ and $S_{o2}(\alpha)$, are Hermitian and positive definite (and hence acceptable as correlation matrices), without those restrictions needing to be explicitly enforced (e.g. through constraints). In fact, any matrix $S \in \mathbb{C}^{d\times d}$ can be additively decomposed into its Hermitian and skew-Hermitian parts: $S = S_1 + S_2$ with $S_1^h = S_1$ and $S_2^h = -S_2$, and we have $\|S\|_F^2 = \|S_1\|_F^2 + \|S_2\|_F^2$. Moreover, it is easy to verify that $G_1 := \mathcal{A}(S_1)$ and $G_2 := \mathcal{A}(S_2)$ are respectively Hermitian and skew-Hermitian. For the objective functional $J(S)$, this gives (since $\hat{G}$ is Hermitian)*

$$2J(S) = \|G_1 - \hat{G}\|_F^2 + \|G_2\|_F^2,$$

so that optimality implies $G_2 = 0$, hence $S_2 = 0$ since by assumption T has full (column) rank. A similar line of reasoning applies to the regularized versions of problem (8).

Remark 4 *From a computational complexity standpoint, both regularizations require $O(md^2) + O(Qd^2) + O(d^3)$ complex arithmetic operations, with $m \gg Q \geq d$ in the present context. The leading $C \times md^2$ amount of arithmetic operations (where C is a method-dependent constant) arises from the decomposition of the transfer matrix T. Both regularization methods may (as explained) use the reduced SVD of T, in which case $C = 6$[23] (Sec. 8.6). Alternatively, the first regularization may as easily be carried out using a thin QR factorization of $[T; \sqrt{\alpha}I]$, resulting in $C = 2$[23] (Sec. 5.2).*

IV. NUMERICAL RESULTS

A. Problem Description

In this section, we demonstrate how we can construct approximate diffuse fields in enclosed rooms for arbitrary frequencies (e.g. below the Schroeder frequency). That is, by driving the room with signals drawn from a multivariate Gaussian vector with zero mean and an optimal speaker correlation, we can obtain a random field in the target region whose spatial cross-correlation is close to (3) in the sense described by (8).

We consider a room with dimensions $5.75 \times 4.25 \times 3\,\mathrm{m}^3$. The impedance for the wall, roof, and floor is taken constant for all simulations and set to $Z = 4.25 \times 10^5\,\mathrm{kg/(m^2\,s)}$, while the speed of sound and mass density are $c = 340\,\mathrm{m/s}$ and $\rho_0 = 1\,\mathrm{kg/m^3}$. The side walls of the room contain uniformly spaced speakers each with an area of $0.25 \times 0.25\,\mathrm{m}^2$. We consider three different speaker configurations in this study: 1) 9 speakers/wall ($d = 36$), 2) 16 speakers/wall ($d = 64$), and 3) 25 speakers/wall ($d = 100$). For each case, we compute optimal speaker correlations for three frequencies: $150, 250$, and 300 Hz. A representative geometry for the room with 36 speakers in shown in Figure 1. The target region, also shown, has dimensions $2 \times 2 \times 2\,\mathrm{m}^3$ and is located in the center of the room.

For each of the studied cases, we first compute a low-rank approximation of the target correlation $\hat{G}$ as per (15), using $Q = 200$. This quadrature rule results in a relative approximation error of less than 0.1% on $\hat{G}$ for all cases studied herein. We then solve the least-squares problems (19) for $1 \leq q \leq Q$. Finally, the optimal speaker cross-correlation S_o is obtained as per (21). The Tikhonov regularization parameter α is determined using an

L-curve approach[24,25]. To this end, we use the objective and regularization term in (22) for either of the regularization strategies described in Section III E. We point out that the computational cost of solving all the aforementioned optimization problems is negligible when compared to the computational cost of building the transfer matrix T.

We use an in-house Finite Element code developed using the FEniCS library[26] in conjunction with the parallel direct solver MUMPS for all the calculations presented herein. The models are meshed with four-node tetrahedral elements. All the results shown are generated with a mesh containing approximately $130,000$ nodes and $750,000$ elements, which is fine enough to achieve a low discretization error in all calculations.

The Schroeder frequency for this room is calculated from (1). The reverberation time is estimated using the Norris-Eyring relation[27]:

$$T_{60} = \frac{-24V\ln(10)}{A\,c\ln(1-\alpha_{rand})},$$

where $A = 2(L_xL_y + L_xL_z + L_yL_z)$ is the room surface area and α_{rand} the random-incidence absorption coefficient[19]

$$\alpha_{rand} = 1 - \int_0^{\pi/2} \left| \frac{Z\cos(\theta) - \rho_0 c}{Z\cos(\theta) + \rho_0 c} \right|^2 \sin(2\theta)\, d\theta.$$

Using the above expressions in (1), we obtain $f_s = 1001$ Hz. Hence, we point out the frequencies used in the examples ($150, 250$, and 300 Hz) are well below the Schroeder limit for this room.

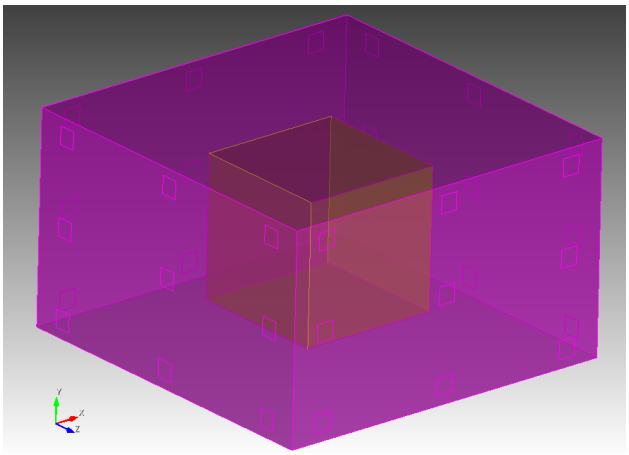

FIG. 1. Room Geometry

B. Results

Let's first define the relative error in correlation (or residual) as

$$\epsilon_G := \frac{\|\mathcal{A}S_o - \hat{G}\|_F}{\|\hat{G}\|_F}$$

Without loss of generality, we use $\frac{p_o^2}{2} = 1$ in all the examples. Hence, a useful metric to explore is how much the diagonal entries of $G^o = \mathcal{A}S_o$ depart from unity. To this end, we define the error

$$\epsilon_{ms} := \frac{\sqrt{\sum_i |G^o_{ii} - 1|^2}}{m}$$

An equivalent interpretation of this error is how much the mean square pressure (normalized to unity in our case) departs from being spatially constant. This is a widely used metric to judge the level of sound diffusion in laboratory experiments[14,15,17] and proved to be very useful for assessing the quality of our numerical solutions.

Table I contains a summary of the results along with the Tikhonov parameter (α) used in each case. We notice that for all frequencies both errors, ϵ_G and ϵ_{ms}, decrease as the number

TABLE I. Results Summary

	150 Hz			250 Hz			300 Hz		
Speakers	ϵ_{ms}	ϵ_G	α	ϵ_{ms}	ϵ_G	α	ϵ_{ms}	ϵ_G	α
36	0.17	0.33	2×10^{-3}	0.35	0.51	1×10^{-2}	0.43	0.64	2×10^{-3}
64	0.09	0.17	1×10^{-3}	0.16	0.30	1×10^{-2}	0.18	0.37	2×10^{-3}
100	0.08	0.16	5×10^{-4}	0.08	0.23	1×10^{-3}	0.08	0.24	5×10^{-4}

of speakers increases, as expected. Another noticeable trend is that these errors increase as frequency increases.

The increasing trend in approximation errors can be explained by studying how the eigenvalues of the target correlation decay as functions of frequency. First, notice that the rank of the approximate correlation, $G_o = TS_oT^h$, is at most d (number of speakers). Hence, using the best approximation error in Eq. (13), we obtain a lower bound for the relative residual of our inverse problem as

$$\frac{\|G_o(d) - \hat{G}\|_F}{\|\hat{G}\|_F} \geq \mathcal{E}(d) \equiv \sqrt{\frac{\sum_{k=d+1}^{m} \lambda_k^2}{\sum_{j=1}^{m} \lambda_j^2}} \tag{25}$$

Hence, we see that the lower bound depends on the decay of the eigenvalue spectrum. To illustrate this behavior in our problem, define a participation factor as

$$P_f^2(d) \equiv \frac{\sum_{k=1}^{d} \lambda_k^2}{\sum_{j=1}^{m} \lambda_j^2}$$

and notice that $\mathcal{E}(d)^2 = 1 - P_f^2(d)$. Now, observe in Fig. 2 how $P_f(d)$ increases with decreasing frequency, in general. The latter trend indicates that the lower bound in Eq. (25)

increases with increasing frequency for a fixed truncation level, which is in agreement with the error trend reported in Table I.

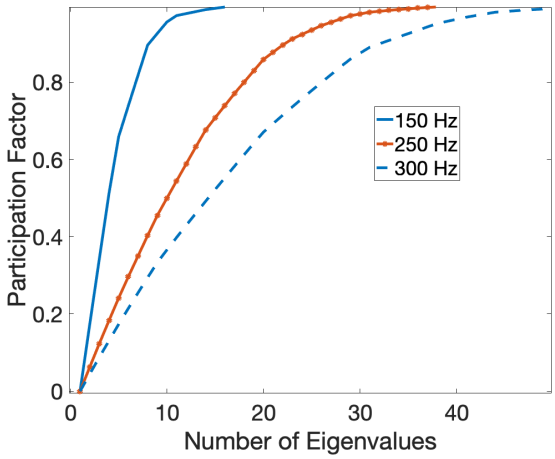

FIG. 2. Participation factor of eigenpairs of the correlation matrix at different frequencies

To better illustrate the quality of our solutions, we plot the correlation field with respect to the center of the target region for different combinations of speakers and frequencies as shown in Figure 3. We can observe that the optimized correlation closely resembles that of a diffuse field. Furthermore, we compare the target and estimated fields along a diagonal across the target region in Figure 4. We can again observe a close match of the computed and target correlations for different frequency and speaker combinations. It is important to point out that we are showing only the target region at the center of the room in these images. As we will show later, the acoustic field departs from being purely diffuse at locations near the walls, as expected.

Recall that the mean square pressure (i.e. diagonal entries of the correlation) is spatially constant in a diffuse field (as captured by the metric ϵ_{ms} shown in Table I). We now provide

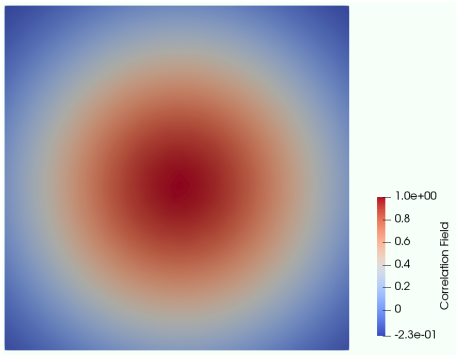

Sinc Function: 150 Hz

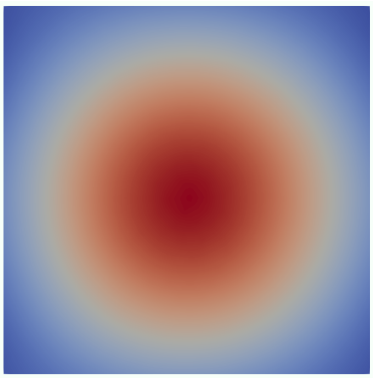

Optimal solution: 150 Hz, 36 speakers

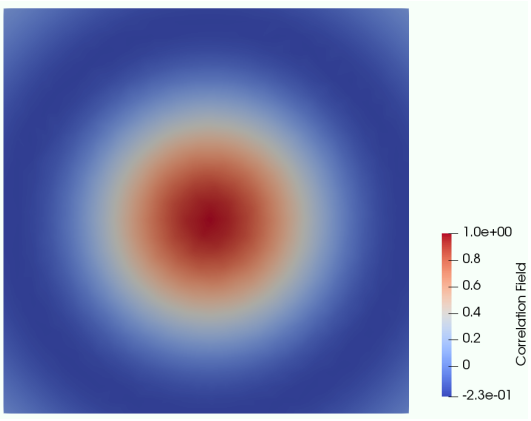

Sinc Function: 250 Hz

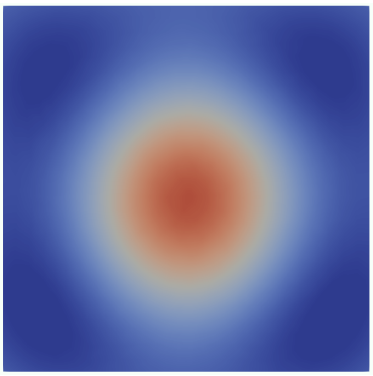

Optimal solution: 250 Hz, 64 speakers

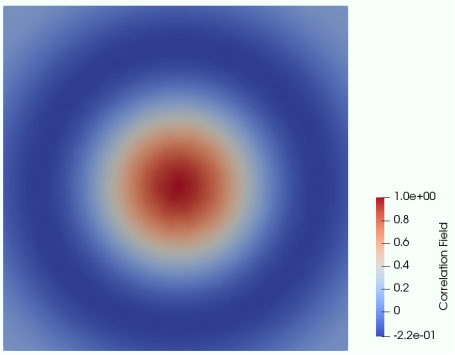

Sinc Function: 300 Hz]

Optimal Solution: 300 Hz, 100 speakers

FIG. 3. Correlation field with respect to the center of the target region.

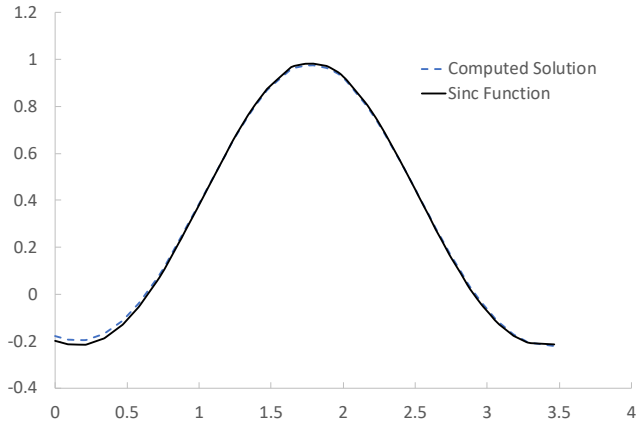

Case: 150 Hz, 36 speakers

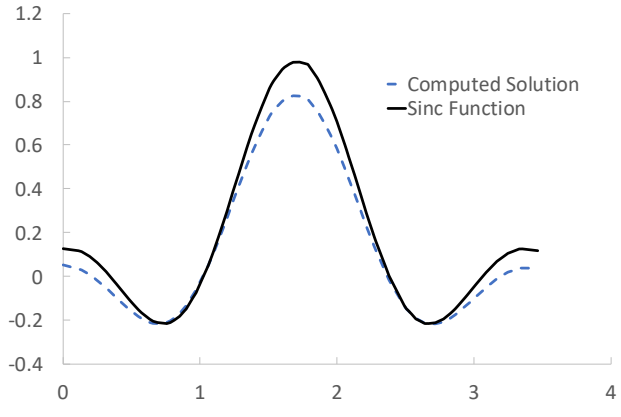

Case: 250 Hz, 64 speakers

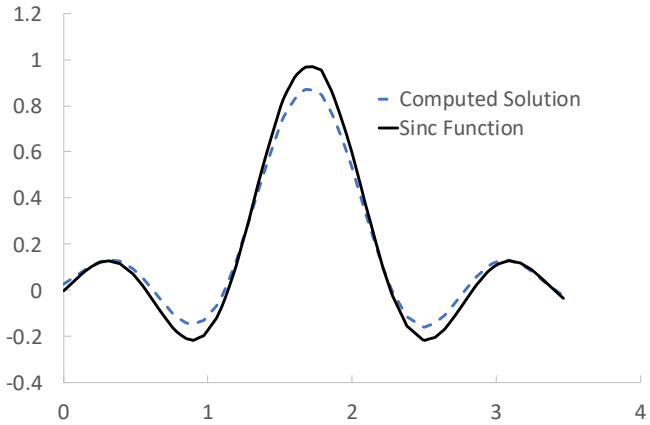

Case: 300 Hz, 100 speakers]

FIG. 4. Correlation field along a diagonal across the target region.

more global representations of this behavior. Figure 5(a) shows the mean square pressure along a line through the center of the room in the X direction for all cases. We can see that the field is close to unity and constant in a region slightly larger than the target domain and departs from pure diffusion close to the walls. Furthermore, for comparison purposes, we show in Figure 5(b) the mean square pressure obtained using random realizations from uncorrelated speakers assuming a standard normal Gaussian distribution. Notice that indeed

uncorrelated speakers cannot produce the desired constant field at this given frequency, reinforcing the success of the proposed optimization approach.

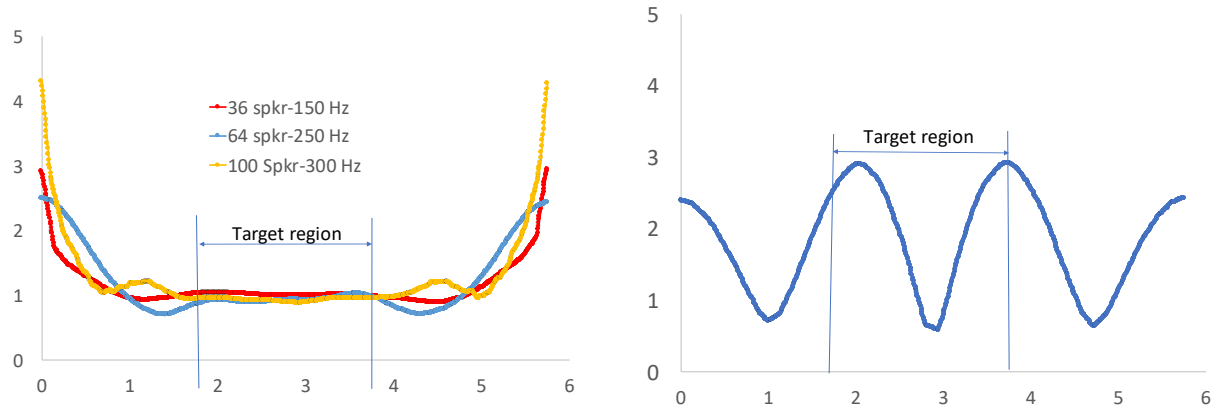

(a) Optimal design cases

(b) Field from 36 uncorrelated speakers at 150 Hz

FIG. 5. Mean square pressure in the entire room along X-axis. Results are normalized to be on the same scale as the optimal case.

Lastly, Figure 6 shows the mean square pressure field for the three studied cases. Again, we notice that, in all cases, the field is constant over a region larger than the target one, but departs from diffuse behavior away from the target region, as expected.

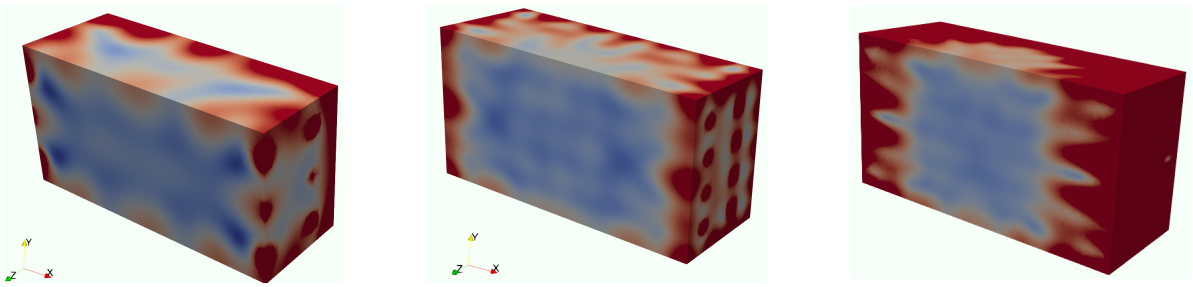

36 spkr-100Hz

64 spkr-250 Hz

100 spkr-300 Hz]

FIG. 6. Mean square pressure in the entire room.

V. SUMMARY AND CONCLUSIONS

We presented how an optimization approach can be used to produce diffuse fields in enclosed rooms at arbitrary frequencies (even below the Schroeder limit). To this end, we characterized a diffuse field solely by its mean and correlation as these are stochastic homogeneous and isotropic Gaussian processes. Then, we postulated an optimization problem in which we sought the correlation structure of input speakers that minimized the distance between the output correlation and that of a diffuse field over a target region. We addressed the large computational cost that arises from the discretization of the target correlation using a low-rank expansion based on the integral representation of spherical Bessel functions. Moreover, we formally showed how to regularize the ensuing ill-posed inverse problem. Our results demonstrated that it is possible to obtain approximate diffuse fields in enclosed rooms even at frequencies below the Schroeder limit by driving correlated speakers in an optimal way. Also, we found that there is a limitation in the quality of the approximation that strongly depends on the number of speakers and the frequencies of interest. As frequency increases a larger number of speakers is needed to maintain a given level of error in the diffuse field approximation. A direction for future work is to study the influence of speaker location on the approximation error. Furthermore, it is possible to devise optimization algorithms to find such locations. Also, incorporating uncertainty in boundary conditions, material properties, etc. in the optimization formulation would be highly desirable.

ACKNOWLEDGMENTS

This work was supported by the Laboratory Directed Research and Development program at Sandia National Laboratories, a multimission laboratory managed and operated by National Technology and Engineering Solutions of Sandia LLC, a wholly-owned subsidiary of Honeywell International Inc. for the U.S. Department of Energy's National Nuclear Security Administration under Contract No. DE-NA-0003525.

REFERENCES

[1]M. Schroeder. Die statistischen Parameter der Frequenzkurven von großen Räumen. *Acustica*, 4:594–600, 1954.

[2]M. R. Schroeder. Statistical parameters of the frequency response curves of large rooms. *J. Audio Eng. Soc.*, 35(5):299–306, 1987.

[3]H. Kuttruff. *Room Acoustics*. Spon Press, 5^{th} edition, 2009.

[4]T. J. Schultz. Diffusion in reverberation rooms. *J. Sound Vibr.*, 16(1):17–28, 1971.

[5]P. A. Larkin and D. O. Smallwood. Control of an acoustical speaker system in a reverberant chamber. Sandia Technical Memo SAND2003-3008C, Sandia National Laboratories, 2003.

[6]F. W. Grosveld and S. A. Rizzi. Controlled reverberant acoustic excitation capabilities at NASA Langley Research Center. 43rd AIAA Aerospace Sciences Meeting, AIAA-2005-0421, January 10-13, 2005.

[7]C. Maury and T. Bravo. The experimental synthesis of random pressure fields: Practical feasibility. *J. Acoust. Soc. Am.*, 120:2712–2723, 2006.

[8]M. Alvarez Blanco, P. Van Vlierberghe, M. Rossetti, K. Janssens, B. Peeters, and W. Desmet. Pre-test analysis to reproduce random pressure fields with multi-channel acoustic control. *Mech. Syst. Signal Proc.*, 163(May 2021):108103, 2022.

[9]S. J. Elliott and J. Cheer. Modeling local active sound control with remote sensors in spatially random pressure fields. *J. Acoust. Soc. Am.*, 137(4):1936–1946, 2015.

[10]S. Zhao, Q. Zhu, E. Cheng, and I. S. Burnett. A room impulse response database for multizone sound field reproduction (l). *J. Acoust. Soc. Am.*, 152(4):2505–2512, 2022.

[11]A.G. de Miguel, M. Alvarez Blanco, E. Matas, H. Bériot, J. Cuenca, O. Atak, K. Janssens, and B. Peeters. Virtual pre-test analysis for optimization of multi-channel control strategies in direct field acoustic testing. *Mech. Syst. Signal Proc.*, 184:109652, 2023.

[12]C. Van Hoorickx and E. P. B. Reynders. Numerical realization of diffuse sound pressure fields using prolate spheroidal wave functions. *J. Acoust. Soc. Am.*, 151(3):1710–1721, 2022.

[13]R. V. Waterhouse. Statistical properties of reverberant sound fields. *J. Acoust. Soc. Am.*, 43(6):1436–1444, 1968.

[14]F. Jacobsen. *The diffuse sound field: Statistical considerations concerning the reverberant field in the steady state*. Acoustics Laboratory, Technical University of Denmark, 1979.

[15]B. Rafaely. Spatial-temporal correlation of a diffuse sound field. *J. Acoust. Soc. Am.*, 107(6):3254–3258, 2000.

[16]M. Grigoriu. *Stochastic Systems: Uncertainty Quantification and Propagation*. Springer Science & Business Media, 2012.

[17]F. Jacobsen and T. Roisin. The coherence of reverberant sound fields. *J. Acoust. Soc. Am.*, 108(1):204–210, 2000.

[18]H. Nélisse and J. Nicolas. Characterization of a diffuse field in a reverberant room. *J. Acoust. Soc. Am.*, 101(6):3517–3524, 1997.

[19]P. M. Morse and K. U. Ingard. *Theoretical Acoustics*. Princeton University Press, 1986.

[20]F. Ihlenburg. *Finite Element Analysis of Acoustic Scattering*. Springer, 1998.

[21]L. Demkowicz. Asymptotic convergence in finite and boundary element methods: Part 1: Theoretical results. *Comput. Math. Appl.*, 27(12):69–84, 1994.

[22]F. W. J. Olver, D. W. Lozier, R. F. Boisvert, and C. W. Clark, editors. *NIST Handbook of Mathematical Functions*. Cambridge, 2010.

[23]G. H. Golub and C. F. Van Loan. *Matrix Computations*. Johns Hopkins University Press, Baltimore, 4^{th} edition, 2013.

[24]P. C. Hansen. Analysis of discrete ill-posed problems by means of the L-curve. *SIAM Review*, 34(4):561–580, 1992.

[25]P. C. Hansen. *Discrete Inverse Problems: Insight and Algorithms*. SIAM, 2010.

[26]M. Alnæs, J. Blechta, J. Hake, A. Johansson, B. Kehlet, A. Logg, C. Richardson, J. Ring, M. E. Rognes, and G. N. Wells. The FEniCS project version 1.5. *Archive of Numerical Software*, 3(100), 2015.

[27]C. F. Eyring. Reverberation time in "dead" rooms. *J. Acoust. Soc. Am.*, 1(2A):217–241, 1930.